Proc. Natl. Acad. Sci. USA
Vol. 92, pp. 2345–2349, March 1995
Biochemistry

DNA structural reorganization upon conversion of a psoralen furan-side monoadduct to an interstrand cross-link: Implications for DNA repair

(NMR/structure/dynamics/photochemistry)

H. PETER SPIELMANN, TAMMY J. DWYER*, SRINIVAS S. SASTRY†, JOHN E. HEARST, AND DAVID E. WEMMER‡

Structural Biology Division, Lawrence Berkeley Laboratory, 1 Cyclotron Road, Berkeley, CA 94720; and Department of Chemistry, University of California, Berkeley, CA 94720

Communicated by Peter G. Schultz, September 6, 1994 (received for review July 12, 1994)

ABSTRACT **We have used ^{1}H NMR spectroscopy to determine the structural changes induced in the DNA oligomer d(5′-GCGTACGC-3′)$_2$ upon conversion of the 4′-hydroxymethyl-4,5′,8-trimethylpsoralen–DNA furan-side monoadduct (MAf) to the interstrand cross-link (XL). The MAf is a photochemical intermediate on the path to interstrand XL and has the psoralen intercalated into the helix. The local DNA structure is distorted in both adducts, but it returns to normal within three base pairs. The formation of XL requires displacement of the psoralen toward the initially unmodified strand, accompanied by a change in the hybridization of the thymine C-5 and C-6 carbons and a change in the local helix twist. The MAf is intercalated in the helix. There is no significant bend in the helix axis of either the MAf or XL. There are significant changes in the local helix dynamics upon photoadduct formation that may be recognized by cellular DNA repair enzyme systems. We hypothesize that the repair enzymes target lesions by detecting the conformational flexibility of the sugar-phosphate backbone induced by DNA-damaging agents.**

Psoralens are a class of photo mutagenic compounds that form covalent nucleic acid adducts through photochemical addition (see Fig. 1) (1–3). The primary reaction is cyclobutane ring formation between the 5,6 double bond of thymidine in DNA and either the 4′,5′ or 3,4 double bond of the psoralen. Reaction at the 4′,5′ double bond creates a furan-side monoadduct (MAf), which can further react at a site with a flanking pyrimidine on the opposite strand to create an interstrand cross-link (XL). Understanding how the DNA deforms to accommodate these adducts is an important part of understanding the sequential two-photon mechanism of XL formation. Data suggest that the mechanism for XL formation (4) is (*i*) intercalation of the psoralen into the DNA, (*ii*) absorption of a long wavelength ultraviolet photon (320–410 nm; UVA) and bond formation to create MAf, (*iii*) conformational changes induced by the adduct formation during a 1-μsec period in which absorption of additional UVA photons does not result in XL formation (5), and (*iv*) absorption of a second UVA photon by the conformationally relaxed MAf and formation of the XL. The photoadducts have a *cis-syn* stereochemistry about the cyclobutane rings determined by the noncovalent intercalation complex. Flow linear dichroism provided evidence for pseudointercalative adduct geometry of the furan-side monoadduct (6), but there have been no detailed structural studies of the reaction intermediate. Both the MAf and XL interfere with replication and transcription and are recognized and efficiently removed by cellular repair enzyme systems (7–13).

The publication costs of this article were defrayed in part by page charge payment. This article must therefore be hereby marked "*advertisement*" in accordance with 18 U.S.C. §1734 solely to indicate this fact.

We have determined the solution structures of the 4′-hydroxymethyl-4,5′,8-trimethylpsoralen (HMT)–DNA furan-side monoadduct and XL intercalated in the 5′-TpA-3′ cross-linkable site of the DNA oligomer d(5′-GCGTACGC-3′)$_2$ using ^{1}H NMR and restrained molecular dynamics (RMD; see Fig. 2). The MAf structure is the post-1 μsec relaxed conformation on the path to XL. Irradiation of the MAf with UVA results in quantitative conversion to XL (14). These structures provide insight into the mechanism of MAf conversion to XL. We describe structural and dynamic properties of the DNA that change upon photoalkylation and the implications that these changes in structure and dynamics may have for cellular DNA repair processes.

MATERIALS AND METHODS

Unmodified (UM) 8-mer MAf, and XL were synthesized and purified as described (14). NMR experiments were performed in 200 mM NaCl, 10 mM deuterated Tris·HCl (pH 7.0), and 0.1 mM sodium EDTA at 25°C on a Bruker AMX 600 spectrometer. MAf heteroduplex was formed by titrating single-stranded octamer MAf with UM as described (15). The oligomer concentrations were 8 mM UM duplex, 8 mM MAf heteroduplex, and 6 mM XL. The numbering scheme for the oligomers is

5′-	G1	C2	G3	T4	A5	C6	G7	C8	-3′
3′-	C16	G15	C14	A13	T12	G11	C10	G9	-5′

NMR spectra of nonexchangeable protons were assigned by standard techniques including nuclear Overhauser effect spectroscopy (NOESY) and double quantum-filtered correlation spectroscopy (DQF-COSY) (16, 17). All HMT, aromatic, and deoxyribose proton (H1′, H2′, H2″, H3′, and H4′) resonances were assigned and in some cases were extended to the H5′/H5″ protons.

NOESY spectra were acquired with mixing times of 25, 50, 100, 175, and 250 msec. Data were processed using FELIX (Biosym Technologies, San Diego). The assigned NOESY crosspeaks were integrated, and the resulting volumes were converted to distance restraints using the iterative relaxation

Abbreviations: HMT, 4′-hydroxymethyl-4,5′,8-trimethylpsoralen; MAf, psoralen–DNA furan-side monoadduct; XL, psoralen–DNA interstrand cross-link; UVA, long wavelength ultraviolet photon (320–410 nm); UM, unmodified; NOESY, nuclear Overhauser effect spectroscopy; DQF-COSY, double quantum-filtered correlation spectroscopy; RMD, restrained molecular dynamics; NOE, nuclear Overhauser effect; AMT, 4′-aminomethyl-4,5′,8-trimethylpsoralen; COSY, correlation spectroscopy.

*Present address: Department of Chemistry, University of San Diego, 5998 Alcala Park, San Diego, CA 92110.
†Present address: The Rockefeller University, 1230 New York Avenue, New York, NY 10021-6399.
‡To whom reprint requests should be addressed.

matrix program MARDIGRAS [University of California, San Francisco (18, 19)]. These distance restraints were incorporated into an RMD procedure. The RMD and energy minimization calculations used DISCOVER (version 2.1), and models were displayed using INSIGHTII (version 2.2.0) (Biosym Technologies). The RMD calculations used the modified assisted model building with energy refinement force-field potentials in DISCOVER. HMT was docked and bonded to a model of either A-form or B-form DNA. The nuclear Overhauser effect (NOE)-derived distance restraints were applied, and the model was energy minimized. This was followed by 20 psec of RMD with the following temperature profile: 200 K for 1 psec warmed to 250 K for 3 psec, then to 300 K for 4 psec, and finally cooled to 100 K in 50 K steps of 3 psec each. The final structure was then energy minimized. Ten structures each were generated for the MAf and XL from both A-form and B-form starting structures. The rms deviation of the 10 structures ranged from 0.4 to 1.2 Å in the MAf and 0.3 to 1.1 Å in the XL. The sum of residual violations of distance restraints for the structures shown were 1.66 Å for the MAf (244 restraints) and 3.38 Å for the XL (226 restraints) with no violation >0.25 Å. A full description of the NMR, data interpretation, and modeling will be reported elsewhere.

RESULTS

Intercalation of the HMT in the MAf is indicated by the interruption of sequential NOEs at the 5′-TpA-3′ step on both strands (20). The T4 to A5 and T12 to A13 assignments were verified by connections through HMT protons. HMT (Fig. 1*A*) is covalently attached to T4 through a cyclobutane ring formed between the 5,6 double bond of the thymidine and the 4′,5′ double bond of the psoralen in the MAf (Fig. 1*B*). Two hundred forty-four NOEs from the central six base pairs and HMT were used in the structure determination of the MAf. The geometry of the T4–HMT adduct with respect to the G3, A5, A13, and T12 nucleotides and the T4 sugar in the MAf helix was defined by 43 NOEs.

XL (Fig. 1*C*) is formed by bonding the HMT MAf to T12 through the 3,4 double bond of the psoralen. Two hundred twenty-six NOEs from the central six base pairs and HMT were used in the structure determination of the XL. The geometry of the T4–HMT–T12 adduct relative to the G3, A5, G11, and A13 nucleotides and the T4 and T12 sugars in the XL helix was defined by 35 NOEs. The covalent structure of the adduct in the XL constrains the relative geometry of T4 and T12.

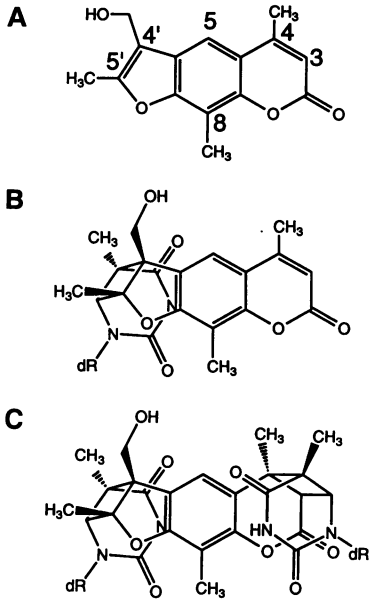

FIG. 1. Structures of HMT (*A*), the *cis-syn* furan-side HMT monoadduct (*B*), and the *cis-syn* HMT cross-link (*C*).

There are a number of structural features common to MAf and XL. The dyad symmetry of the UM DNA is broken by the photochemical alkylation of the HMT in each, but the terminal residues of the DNA are spectroscopically degenerate for both. The penultimate residues of both the MAf and the XL are nearly degenerate and are equivalent in chemical shift to UM DNA. This indicates that the DNA structure in the MAf and XL returns to normal B-form DNA within three base pairs of the adduct. The helix parameters for the penultimate base pairs in the MAf and XL are consistent with B-form DNA. The terminal base pairs were modeled as B-form DNA because DQF-COSY and NOESY results indicate that they are frayed and undergoing conformational exchange in the MAf, XL, and UM DNA (21). Normal Watson–Crick hydrogen bonding is present in the UM DNA, MAf, and XL, except for the T12·A5 base pair in the XL for which the imino resonance is broad, indicating increased solvent accessibility (22). The hydrogen bonds of the adducted thymidine residues are distorted away from their ideal geometries in both the MAf and the XL.

The helix is unwound by 28° and has an overall helical repeat of 11 base pairs in both the MAf and the XL, which is consistent with intercalation of the HMT (23). Helix parameters were calculated with the program CURVES (24, 25); a more detailed analysis and distribution will be described elsewhere. The MAf helix is unwound by 27° at the thymidine and adenine base step as a result of the insertion of the psoralen. The underwinding in the MAf is distributed over the G3/T4, T4/A5, A5/C6, and C6/G7 steps. The thymidine–adenosine base step in the XL is overwound to 39° due to the covalent geometry imposed on the DNA by the HMT cross-link. The overwinding at the XL T4/A5 step is compensated for by the underwinding of the C2/G3, G3/T4, and A5/C6 steps. The DNA deforms locally in response to formation of both the MAf and the XL.

MAf Description. The HMT adduct does not extend all the way across the helix in the MAf, and T12 rolls slightly into the major groove to maximize van der Waals contacts with the pyrone ring of the HMT (Fig. 2 *Left*). The modified T4 forms an imperfect stack with the neighboring base G3. Cyclobutane ring formation changes the hybridization of carbons 5 and 6 of T4 from sp^2 to sp^3, forcing the methyl group (5-Me) and 6-H of the adducted thymidine away from the HMT. The adjacent guanine stacks onto the surface formed by the adducted T 5-Me, 6-H, and pyrimidine ring, which is much less tilted than the pyrimidine ring alone (Fig. 3). Although the thymidine buckles in response to monoadduct formation, the base pairing of the adducted thymidine with A13 does not appear to be appreciably disturbed, as indicated by imino proton exchange.

A minor bend in the helix axis is introduced into the DNA by the MAf (≈8° overall). The MAf helix axis is not kinked by the adduct because A5 and A13 remain coplanar with the HMT. G3 of the MAf is rolled slightly into the major groove contributing to the small bend into the major groove. We believe that bends of this magnitude cannot be accurately determined with current NMR methods and are difficult to measure with any technique. The presence or absence of a small bend induced by the MAf might be more reliably measured by other techniques, such as gel mobility assays, which are beyond the scope of the present work.

XL Description. The formation of the XL introduces a large buckle into the T4·A13 and T12·A5 base pairs. The helix axes of the MAf and the XL are coincident when the molecules are superimposed, and again the helix axis is not bent by the XL (≈0° overall). Cross-link formation can be accommodated without kinking because A5 and A13 remain coplanar with the HMT. G3 stacks onto the 5-Me and modified ring of T4, and G11 stacks onto the 5-Me and modified ring of T12 coplanar with the HMT in the XL (Fig. 2 *Right*). This is in contrast to

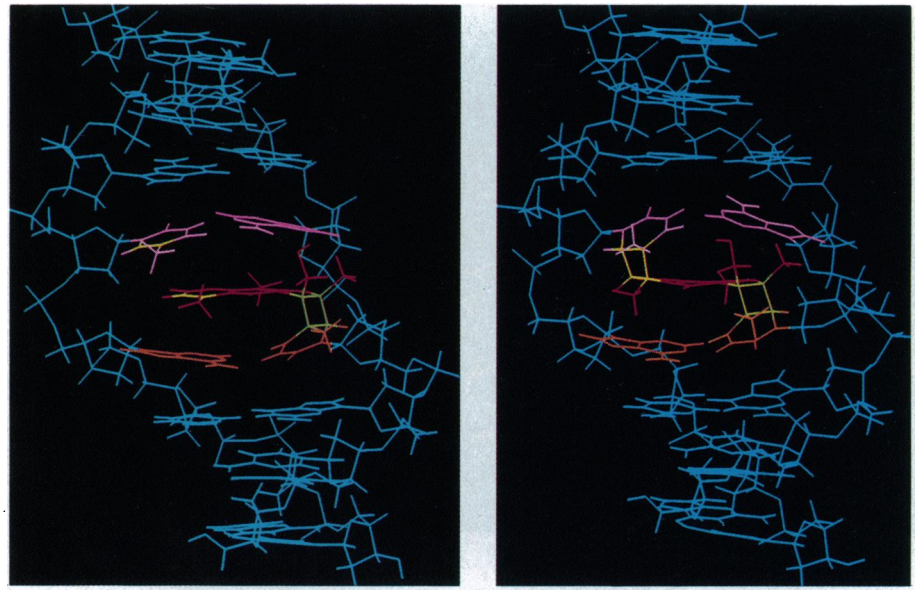

FIG. 2. Structures of the MAf and the XL. (*Left*) MAf looking into the major groove. The HMT is shown in red, the adducted T4·A13 base pair is in orange, the furan-side cyclobutane ring is in green, the T12·A5 base pair is in pink, and the atoms that will form the pyrone-side cyclobutane are in yellow. (*Right*) XL looking into the major groove. The HMT is shown in red, the T4·A13 base pair is in orange, the furan-side cyclobutane ring is in green, the T12·A5 base pair is in pink, and the pyrone-side cyclobutane ring is in yellow.

the previously reported structure for the 4′-aminomethyl-4,5′,8-trimethylpsoralen (AMT)–d(5′-GGGTACCC-3′)$_2$ cross-link for which a sharp 56° kink was reported at the site of the adduct (26). A similar kink was suggested by a theoretical model of double-stranded DNA containing an interstrand cross-link based on the x-ray crystal structure of the 8-methoxypsoralen thymine furan-side monoadduct (27). Bending of psoralen cross-linked DNA observed by EM has been explained in terms of increased flexibility of the DNA around the site of an XL adduct (28). Our results for the structures of the MAf and XL are in agreement with gel shift results for psoralen-modified DNA (29, 30), do not contradict the EM data, and represent a correction of the earlier structure. There are at least two technical factors that contributed to the problems with the AMT-XL structure that are unrelated to the differences in the psoralen and DNA sequence. The contribution of spin diffusion to the NOE intensities was not accounted for in the AMT-XL system, and the AMT-XL structure was refined without RMD from a bent starting model, introducing a conformational bias. Detailed reasons for the discrepancy with the earlier model will be discussed elsewhere.

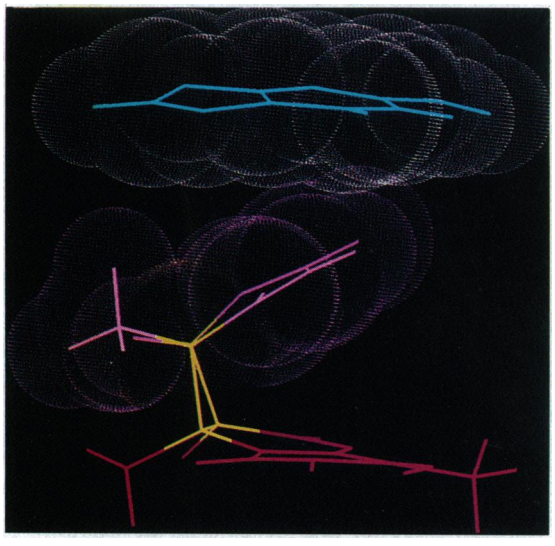

FIG. 3. van der Waals stacking interaction between G11 and T12 in the XL. The G11 van der Waals surface is shown in white, and T12 van der Waals surface is shown in pink. The HMT is in red and the pyrone-side cyclobutane ring is in yellow.

DISCUSSION

Structural Reorganization in the Adducts. The main features that relate the MAf and the XL structures to the photochemical mechanism are (*i*) intercalation of the psoralen between the bases at the 5′-TpA-3′ step, (*ii*) a substantial local conformational change in the DNA when MAf is converted to XL, (*iii*) unwinding of the DNA helix as a result of the intercalation of the adducts, (*iv*) the return of the DNA to B-form geometry within three base pairs of the site of damage, (*v*) the absence of a significant bend in the helix axis for either MAf or XL, and (*vi*) destabilization of the C2′ endo conformation of the deoxyribose sugar residues at the site of photoadduction.

There are no direct data available for the structure of the noncovalent complex of HMT with DNA. No changes in the NMR spectrum occur upon titration of UM DNA with HMT, which is not surprising because HMT is only soluble to 0.16 mM in water and has a relatively high K_d of 2.9×10^{-4} (4). Previous experiments with the structurally related AMT indicated that there was no sequence specificity for the initial noncovalent complex (26). Absorption of a photon by the psoralen intercalated at the correct site yields the furan-side monoadduct.

The MAf must arise from an HMT bound in a parallel intercalation geometry, similar to the NMR-derived MAf structure, based on the transition state for the cyclobutane ring formation. This is in agreement with calculations for 8-methoxypsoralen, which predict a parallel intercalation mode and that the furan ring of the psoralen is closer to the pyrimidine 5,6 bond than is the pyrone ring (31). After the absorption of a photon by the intercalated HMT, the internuclear bond distances for the atoms involved in the cyclobutane ring shorten, forcing the thymidine methyl group into the neighboring base by the change in hybridization from sp^2 to sp^3 at

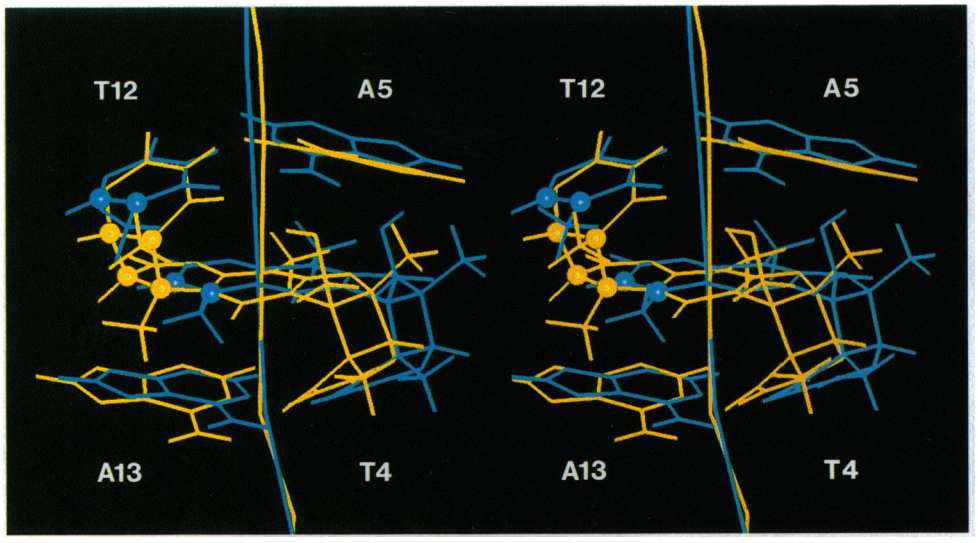

FIG. 4. Stereoview of the TpA site superimposition of the MAf and XL showing conformational changes upon XL formation. The MAf is shown in yellow and the XL is in blue. The atoms that form the pyrone-side cyclobutane ring are highlighted as balls. The helix axis runs through the center of the adduct.

the affected carbons. These changes in geometry occur during the 1-μs period before the adduct can form XL.

The present structural analysis allows us to examine the conformational changes that occur when the MAf is photochemically converted to XL. The 3.47 Å separation of T12 C-5 and MAf C-4 and the 3.35 Å separation of T12 C-6 and MAf C-3 change to 1.54 Å each upon XL formation. The MAf–T4 adduct moves 1.5 Å into the major groove relative to the helix axis (Fig. 4). T12 rolls down toward the HMT when the pyrone-side cyclobutane ring is formed, but it is not displaced relative to the helix axis. The HMT shifts into the major groove and across the helix axis toward T12 upon cross-link formation. The A5 amino group stacks onto the benzene ring of the HMT in the MAf and onto the furan ring of the HMT in the cross-link (Fig. 5). A5 moves 1.0 Å toward the major groove upon cross-link formation and rolls slightly into the minor groove because of a steric clash between the amino group and the 4′-hydroxymethyl of the HMT. The HMT 8-methyl in both the MAf and XL is stacked onto the six-membered ring of A5. A13 moves slightly into the minor groove when the 4-methyl of the HMT clashes with the five-membered ring of A13 upon cross-link formation. A5 and A13 form an almost coplanar stack with the HMT in both the MAf and XL. The hydrogen-bonding edge of T12 is rotated into the major groove by cyclobutane ring formation when the MAf is converted to XL. This exposes the T12 imino proton, leading to more rapid solvent exchange and potentially destabilizes the T12·A5 base pair in the XL.

Implications for DNA Repair. Excision repair systems efficiently recognize and remove many structurally diverse DNA-damaging agents, including psoralen, whereas the wide range of normal DNA microstructures do not trigger any response (32). Recognition of DNA damage by these systems has been proposed to take place by the detection of structural changes and/or the alteration of the dynamic behavior of the DNA (8, 33, 34). It has been proposed that damage causes local instability in the helix and that the (A)BC excision repair system recognizes this excessive or unusual deformability (35). We have compared the conformations of the UM sugars with those of MAf and XL to investigate whether psoralen damage induces changes in conformational dynamics in the DNA. Deoxyribose sugar conformations can be obtained by analysis of the fine structure of two-dimensional correlation spectroscopy (COSY) crosspeaks (36, 37). We used soft-COSY techniques to determine the sugar conformations for T4 and A5 in UM DNA and T12 and A13 in the MAf (15). Sugar conformations were measured with high accuracy by fitting selective COSY data acquired with high digital resolution to a two-state model for the deoxyribose conformations (15, 38). T4 and A5 in the UM DNA are in the normal range for DNA conformations ≥70% C2′ endo. In contrast, we were unable to fit the data for the MAf T12 and the MAf A13 sugar conformations

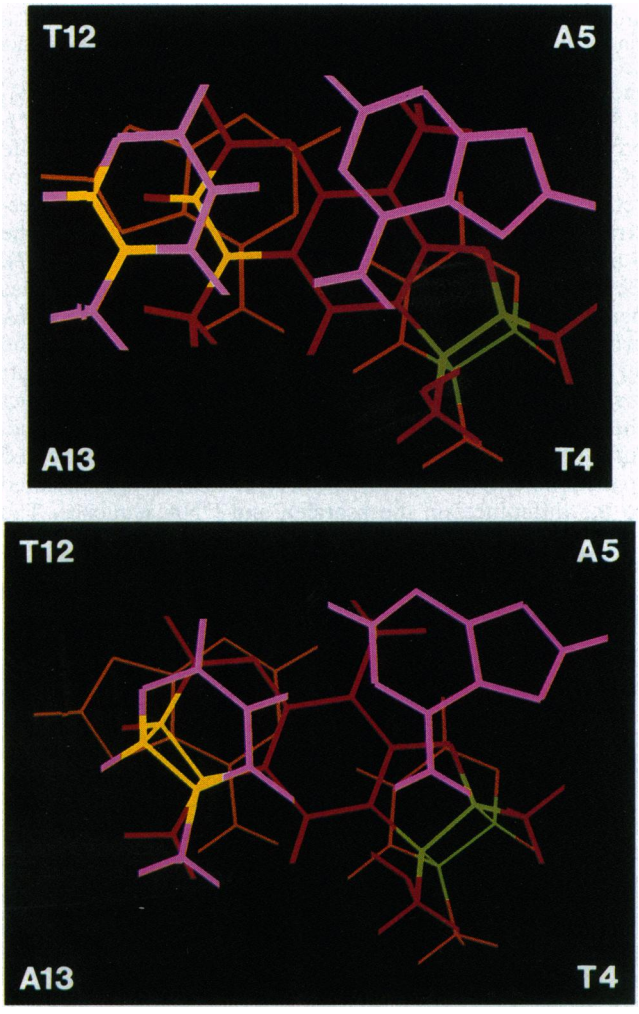

FIG. 5. Stacking interactions and intercalation geometry of the HMT and bases of the TpA step viewed down the helix axis. (*Upper*) The MAf and the XL (*Lower*) are shown. The A5·T12 base pair is on top shown in pink, followed by the HMT in red and the T4·A13 base pair at the bottom in orange. The furan-side cyclobutane ring is in green, and pyrone-side cyclobutane ring forming atoms are shown in yellow.

to the simple two-state model, indicating more complex dynamic behavior. These residues are on the unmodified strand of the MAf duplex.

The deoxyribose 1′-2′ and 1′-2″ crosspeaks of C2 and C6 of the UM DNA and C2, C6, C10, and C14 in both the MAf and the XL have the same qualitative structure as the corresponding UM DNA T4 and A5 crosspeaks in low digital resolution DQF-COSY spectra. We believe that these sugar residues are predominantly C2′ endo by analogy with the selective COSY results for the UM T4 and A5. The deoxyribose 1′-2′ and 1′-2″ cross-peaks of A5 in the MAf and the XL are similar in structure to the MAf T12 cross peaks, indicating that these residues have complex mixtures of conformations. The structure of the 1′-2′ and 1′-2″ crosspeaks of T4 in the MAf and the XL could not be matched to either simulated spectra for any one sugar conformation of the structure of the MAf T12 cross-peaks (36). The DQF-COSY crosspeaks for the remaining sugar residues were not amenable to this analysis due to spectral overlap. We believe that the HMT damage destabilizes the preference for C2′ endo sugar conformation of the four nucleotides (T4, A5, T12, and A13) involved in or adjacent to the adducts, permitting them to adopt a larger range of rapidly interconverting conformers with a significantly altered population distribution with respect to UM DNA.

The initial strand incision made by the (A)BC exinuclease complex preferentially cuts the DNA on the furan side of an HMT interstrand XL. There is a lower specificity for the initial strand incision for the furan vs. pyrone side in the case of trimethylpsoralen–thymidine cross-links (39). This has been suggested to be a consequence of the presence of the 4′-hydroxymethyl group in HMT (7). The data are insufficient at this time to show differences in the dynamic properties of the two strands in the HMT XL. When the MAf of HMT is converted to XL, a steric clash with the amino group of A5 develops, which forces that base to be slightly displaced into the minor groove. A less severe steric interaction would be expected with the 4′ proton of trimethylpsoralen. The different magnitude of the displacement of A5 in the two molecules may modulate the changes in dynamics observed for the sugars, which in turn may be differentially recognized by the repair complex.

The coupled "crankshaft motions" of the phosphate backbone and motion of the bases related to the dynamic conformational changes in the deoxyribose observed in the MAf and the XL may be recognized as a signal by the DNA repair systems to locate DNA damage. The DNA repair system in this model recognizes changes in the equilibrium behavior of the DNA surrounding the adduct, not specific structural features induced by the damage. Other DNA oligomers covalently modified with drugs that are recognized by cellular repair systems and have radically different structures from the MAf and the XL show evidence of altered helix dynamics by NMR (40). We hypothesize that the repair enzymes target lesions by detecting the conformational flexibility of the sugar-phosphate backbone induced by DNA-damaging agents. There are numerous amino acid contacts to the backbone phosphates observed in high-resolution x-ray crystal structure of protein–DNA complexes (41). The flexibility of the phosphate esters in the recognition and formation of protein–DNA contacts has been proposed as a mechanism for discrimination of different operator sites by the *lac* repressor (42, 43). Flexibility of the backbone is a more general case of localized sequence-specific conformational variations in DNA that are potentially recognized by proteins. It is possible that excision repair systems recognize a dynamic coupling between the protein and the DNA that is sensitive to the greater conformational freedom of the backbone of damaged DNA. Further experiments that look directly at the geometry and dynamics of the backbone will be required to prove these assertions.

This work was supported in part by National Institutes of Health Grant GM-43219 (D.E.W.); postdoctoral fellowship GM-14966 (H.P.S.); through instrumentation grants from the U.S. Department of Energy (DE FG05-86ER75281) and the National Science Foundation (DMB 86-09305 and BBS 87-20134); by the Director, Office of Energy Research, Office of Basic Energy Sciences, Materials Sciences Division of the U.S. Department of Energy under Contract no. DE-AC03-76SF00098 (J.E.H.), and by the Director, Office of Biological and Environmental Research, General Sciences Division of the U.S. Department of Energy under Contract no. DE-AC03-76SF00098 (D.E.W.).

1. Straub, K., Kanne, D., Hearst, J. E. & Rapoport, H. (1981) *J. Am. Chem. Soc.* **103,** 2347–2355.
2. Kanne, D., Straub, K., Hearst, J. E. & Rapoport, H. (1982) *J. Am. Chem. Soc.* **104,** 6754–6764.
3. Kanne, D., Straub, K., Rapoport, H. & Hearst, J. E. (1982) *Biochemistry* **21,** 861–871.
4. Isaacs, S. T., Shen, C.-K. J., Hearst, J. E. & Rapoport, H. (1977) *Biochemistry* **16,** 1058–1064.
5. Johnston, B. H., Johnson, M. A., Moore, C. B. & Hearst, J. E. (1977) *Science* **197,** 906–908.
6. Vigny, P., Blais, J., Ibanez, V. & Geacintov, N. E. (1987) *Photochem. Photobiol.* **45,** 601–607.
7. Cheng, S., Sancar, A. & Hearst, J. E. (1991) *Nucleic Acids Res.* **19,** 657–663.
8. Sancar, A. & Sancar, G. B. (1988) *Annu. Rev. Biochem.* **57,** 29–67.
9. Smith, C. A. (1988) in *Psoralen DNA Photobiology*, ed. Gasparro, F. P. (CRC, Boca Raton, FL), pp. 87–116.
10. Smith, K. C., Wang, T.-c. V. & Sharma, R. C. (1989) *BioEssays* **10,** 12–16.
11. Sladek, F. M., Munn, M. M., Rupp, W. D. & Howard-Flanders, P. (1989) *J. Biol. Chem.* **264,** 6755–6765.
12. Van Houten, B., Gamper, H., Holbrook, S., Sancar, A. & Hearst, J. E. (1986) *Proc. Natl. Acad. Sci. USA* **83,** 8077–8081.
13. Van Houten, B., Gamper, H., Sancar, A. & Hearst, J. E. (1988) *J. Biol. Chem.* **263,** 16553–16560.
14. Spielmann, H. P., Sastry, S. S. & Hearst, J. E. (1992) *Proc. Natl. Acad. Sci. USA* **89,** 4514–4518.
15. Emsley, L., Dwyer, T. J., Spielmann, H. P. & Wemmer, D. E. (1993) *J. Am. Chem. Soc.* **115,** 7765–7771.
16. Hare, D. R., Wemmer, D. E., Chou, S.-H., Drobny, G. & Reid, B. R. (1983) *J. Mol. Biol.* **171,** 319.
17. Wüthrich, K. (1986) *NMR of Proteins and Nucleic Acids* (Wiley, New York).
18. Borgias, B. A. & James, T. L. (1988) *J. Magn. Reson.* **79,** 493.
19. Borgias, M., Gochin, M., Kerwood, D. J. & James, T. L. (1990) *Prog. Nucl. Magn. Reson. Spectrosc.* **22,** 83–100.
20. Zhang, X. & Patel, D. J. (1991) *Biochemistry* **30,** 4026–4041.
21. Schmitz, U., Sethson, I., Egan, W. M. & James, T. L. (1992) *J. Mol. Biol.* **227,** 510–531.
22. Patel, D. J., Pardi, A. & Itakura, K. (1982) *Science* **216,** 581–590.
23. Wiesehahn, G. P. & Hearst, J. E. (1978) *Proc. Natl. Acad. Sci. USA* **75,** 2703–2707.
24. Lavery, R. & Sklenar, H. (1988) *J. Biomol. Struct. Dyn.* **6,** 63–91.
25. Lavery, R. & Sklenar, H. (1989) *J. Biomol. Struct. Dyn.* **6,** 655–667.
26. Tomic, M., Wemmer, D. & Kim, S. H. (1987) *Science* **238,** 1722–1725.
27. Pearlman, D. A., Holbrook, S. R., Pirkle, D. H. & Kim, S.-H. (1985) *Science* **227,** 1304–1308.
28. Shi, Y., Griffith, J., Gamper, H. & Hearst, J. E. (1988) *Nucleic Acids Res.* **16,** 8945–8952.
29. Sinden, R. R. & Hagerman, P. J. (1984) *Biochemistry* **23,** 6299–6303.
30. Haran, T. E. & Crothers, D. M. (1988) *Biochemistry* **27,** 6967–6971.
31. Demaret, J.-P., Brunie, S., Ballini, J. P. & Vigny, P. (1989) *Photochem. Photobiol.* **50,** 7–21.
32. Lin, J. J. & Sancar, A. (1992) *Mol. Microbiol.* **6,** 2219–2224.
33. Lin, J. J. & Sancar, A. (1989) *Biochemistry* **28,** 7979–7984.
34. Pu, W. T., Kahn, R., Munn, M. M. & Rupp, W. D. (1989) *J. Biol. Chem.* **264,** 20697–20704.
35. Williams, L. D. & Gao, Q. (1992) *Biochemistry* **31,** 4315–4324.
36. Gochin, M., Zon, G. & James, T. L. (1990) *Biochemistry* **29,** 11161–11171.
37. Ernst, R. R., Bodenhausen, G. & Wokaun, A. (1987) *Principles of Nuclear Magnetic Resonance in One and Two Dimensions* (Clarendon, Oxford, U.K.).
38. Rinkel, L. J. & Altona, C. (1987) *J. Biol. Struct. Dyn.* **4,** 621–649.
39. Jones, B. K. & Yeung, A. T. (1990) *J. Biol. Chem.* **265,** 3489–3496.
40. O'Handley, S. F., Sanford, D. G., Xu, R., Lester, C. C., Hingerty, B. E., Broyde, S. & Krugh, T. R. (1993) *Biochemistry* **32,** 2481–2497.
41. Beamer, L. J. & Pabo, C. O. (1992) *J. Mol. Biol.* **227,** 177–196.
42. Karslake, C., Botuyan, M. V. & Gorenstein, D. G. (1992) *Biochemistry* **31,** 1849–1858.
43. Botuyan, M. V., Keire, D. A., Kroen, C. & Gorenstein, D. G. (1993) *Biochemistry* **32,** 6863–6874.